Critical comparison of interfacial boundary conditions in modelling plasma-liquid interaction

Pepijn Heirman and Annemie Bogaerts

Research group PLASMANT, Department of Chemistry, University of Antwerp, Antwerp, Belgium

e-mail: pepijn.heirman@uantwerpen.be

Abstract

Several computational models have been developed over the past decade with the goal to investigate the various processes that occur during plasma-liquid interaction. However, many different boundary conditions to describe transfer of chemical species over the gas-liquid interface have been reported in these investigations. In this work, we employ a computational model to test these various boundary conditions, and compare the results to experimental data for H_2O_2, O_3, $\cdot NO$ and HNO_2, in order to assess how well these boundary conditions can describe the dissolution of different species. We show that the validity of the different formulas depends on the solubility of the investigated chemical species; they appear valid for species with high solubility (H_2O_2), but not for species with low (O_3 and $\cdot NO$) or intermediate (HNO_2) solubility. Finally, we propose an approach to reach better agreement, based on film theory in combination with the mass accommodation coefficient.

1. Introduction

The treatment of a liquid with (non-thermal) plasma is a research subject that is steadily gaining interest. Several promising applications are being investigated, ranging from agriculture and nitrogen fixation (1), to water treatment (2-4) and plasma medicine (5, 6). In the latter, treatment of cells is most often investigated *in vitro*, where the treated cells are covered by a liquid layer, such as cell medium (7, 8). In general, the main effects of plasma treatment in these applications, be it the degradation of a pollutant for water purification, killing of cancer cells in plasma oncology, or stimulation of cells in wound healing, are induced by the reactive oxygen and nitrogen species (RONS) produced by the plasma. These species are produced in the plasma and diffuse into the treated liquid (9), where they can further react with each other, or with components already present in the liquid.

Many phenomena are at play during interaction between plasma and liquid (10), as both phases continuously influence each other during treatment (11, 12). This makes experimental research into such a system challenging. Indeed, understanding of the transport processes at the plasma-liquid interface is consistently pointed out as a major challenge (10, 13-15). Next to experimental research, computational simulations can form a valuable tool to elucidate the various processes that occur during plasma-liquid interaction. Over the past decade, several computational models have been developed, with varying degrees of complexity, to investigate the plasma treatment of a liquid and, specifically, the reactive chemical species that end up in the liquid upon treatment. For example, Verlackt *et al.* (16) developed a 2D axisymmetric model to investigate transport phenomena during treatment of a liquid-filled beaker with

a plasma jet. Kruszelnicki et al. (17) reported on the simulation of the treatment of water droplets with air plasma, using both a 0D model and 2D model. Semenov et al. (18) presented a modelling study focusing on the description of convection and diffusion in a plasma-liquid system. Integral to a computational model that simulates plasma-liquid interaction is the description of the dissolution of reactive species from the gas phase into the liquid phase. Notably, each of the computational works discussed above employs a different method of describing this species transfer across the plasma-liquid interface.

Physically, the solubility of gas in a liquid is described by Henry's law (19):

$$\frac{c_l}{p} = H^{cp} \tag{1}$$

Where H^{cp} is the Henry's law solubility constant of the chemical species, c_l is the concentration of the species in the liquid phase, and p is its partial pressure in the gas above the liquid. Henry's law is, however, an equilibrium law, i.e. it describes the concentration of species in the gas and liquid phase in steady state, and does not give any information on the rate of the dissolution process, i.e. how fast this equilibrium is reached. Moreover, before steady state is reached, phenomena can arise that complicate things further, such as the depletion of a soluble gaseous species near the liquid interface. Different published models simulating plasma-liquid interaction have used a variety of boundary conditions at the plasma-liquid interface, to describe species transfer between both phases in a way that adheres, if steady state is reached, to Henry's law. Often, however, comparison of the liquid concentrations to experimental data, which would support the use of these boundary conditions, is lacking. In the few cases where simulation results on the predicted dissolution of reactive species have been benchmarked against experiments, this was done only for H_2O_2, which has a high solubility. Of course, experiments that can test the validity of the boundary condition describing solvation, independently of other factors such as chemical reactions, are not straightforward. For a few cases, though, experimental data has been published (20, 21).

In this work, we employ our recent computational model, presented in (22), to investigate and compare the various expressions for the description of species transfer between gas and liquid, as used in published computational works in the field of plasma-liquid interaction. The results are compared to published experimental data, in order to assess how well these expressions are able to replicate experimental results, a crucial prerequisite for the use of a computational model to both explain and predict experimental outcomes. To the best of our knowledge, no critical comparison of these expressions, benchmarked with experimental data, is available in literature until now. Our data indicates that the validity of the different formulas depends on the solubility of the investigated chemical species, and that none of the tested expressions is able to replicate experimental data for all species. Finally, we expand our view to fields outside plasma-liquid interaction, and propose an approach to reach better agreement.

2. Methods

2.1 Computational model

We use a 2D-axisymmetric model of a (plasma) jet above liquid water, describing both the gas and liquid phase, presented in (22). Briefly, the model, built with the software COMSOL Multiphysics (version 6.2), first calculates the stationary state of the flow field in the simulated system by solving the time-independent, incompressible Navier-Stokes equations, employing Menter's shear stress transport (SST) model to account for turbulence. At the stationary gas-liquid interface, of which the shape is based on observations in our lab (unless specified otherwise), the gas flow sets the liquid in motion through continuity of flow velocity and shear stress. As the velocity field greatly affects transport of gaseous species towards the liquid, and is crucial for determining transport of dissolved species in the liquid phase, we have benchmarked our description of the velocity field by comparing our model to the experimental data reported by Stancampiano *et al*. (23), showing good agreement. These results can be found in the **Appendix**.

Using this flow field as input, the temperature and chemical species transport in the system are calculated, fully coupled, by solving for the conservation of energy and mass in a time-dependent manner. The plasma and its corresponding chemistry are not included in the simulations, which is not needed for the current investigation, as the experimental data used for benchmarking also did not include an ignited plasma. At the gas-liquid interface, temperature is continuous. Evaporation of water is calculated via Antoine's law, although it is assumed that the liquid volume remains unchanged, while the accompanying evaporative cooling of the liquid is accounted for.

Each of the various expressions tested throughout this work to describe dissolution of RONS into the treated liquid at the gas-liquid interface, which are discussed in detail in **section 3.2**, depends on Henry's constant of the simulated species. We employ the temperature-dependent Henry's constant, calculated as follows (19):

$$H^{cp} = H^{cp,0} \cdot \exp\left(\frac{-\Delta_{sol}H}{R}\left(\frac{1}{T} - \frac{1}{T^0}\right)\right)$$

(2)

Where $H^{cp,0}$ is the Henry's constant at the standard temperature $T^0 = 298.15$ K, $\Delta_{sol}H$ is the enthalpy of dissolution (J/mol), and R is the gas constant (J/mol·K). The parameters in **equation 2** are taken from (19), and are shown in **Table 1**.

Table 1: Parameters used to calculate the temperature-dependent Henry's constants of RONS used in this work.

Species	$H^{cp,0}$ (mol/m³·Pa)	$\frac{-\Delta_{sol}H}{R}$ (K)
H_2O_2	8.6×10^{2}	7300
O_3	1.0×10^{-4}	2800
$\cdot NO$	1.9×10^{-5}	1600
HNO_2	4.7×10^{-1}	4900

Note that the temperature-dependence of the Henry's constant is in fact not linear. However, for the simulated conditions, the above expression is sufficient (24).

2.2 Model geometries

Figure 1 shows the different model geometries used throughout our investigation, each based on an experimental setup reported in literature. To mimic the experimental data as close as possible, each simulation is performed for the same conditions as those described in the respective literature, including the working gas composition and inlet flow rate. The geometry shown in **Figure 1a** is based on the setup used by Winter *et al.* (20), where a petri dish containing 5 mL liquid was treated with the kINPen plasma jet, without igniting the plasma, with a gap between the jet nozzle and the liquid surface (before treatment) of 9 mm. Through the jet inlet, 3 standard liters per minute (SLM) of humid argon containing 5 ppm H_2O_2 enters the gas phase domain. The shielding gas inlet has a flow rate of 5 SLM dry air. It is stated in (20) that the kINPen was continuously moved over the liquid during treatment, mixing the liquid. Hence, the liquid phase is assumed to be well mixed, as in (18).
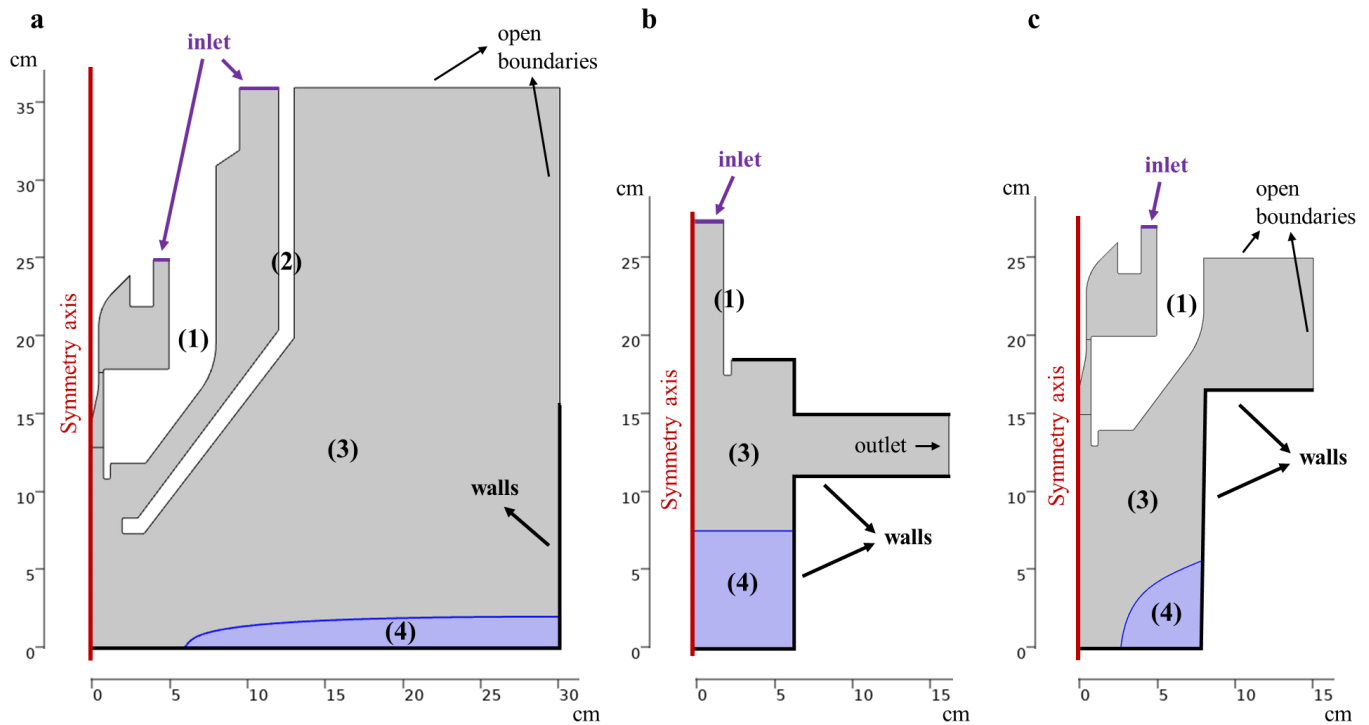

Figure 1: Model geometries used throughout the present work, based on the experimental setups used in (20) (a), (21, 25) (b), and (26) (c). The geometry components are (1) the jet, (2) the shielding gas device (when present), (3) the gas phase and (4) the liquid phase. Boundary conditions at the model edges are indicated, including the symmetry axis around which the 2D axisymmetric model is revolved. Note that in (a) and (c) the liquid is pushed away by the gas to such a degree that the gas reaches the bottom of the petri dish or well.

Figure 1b represents the geometry based on the setup of Hassan *et al.* (21, 25). Either 1000 µL (as shown here) or 500 µL is treated with either 2 SLM of 50 % humid air containing 110 ppm H_2O_2, 1.6 SLM of dry air containing 450 ppm O_3, or 1 SLM of humid air containing 100 ppm HNO_2. The gas-liquid interface is flat, based on the observations described in (21), and has the same surface area for both liquid volumes (i.e.,

only the liquid depth is changed). Unlike for the other geometries, laminar flow is simulated in the gas phase because of the much lower flow velocity. For this geometry, the outlet tube in our model is an approximation, as this element of the experimental setup is not axisymmetric.

Finally, the geometry in **Figure 1c** represents the experimental setup used by Jablonowski *et al.* (26), where a 24 well plate containing 750 µL of liquid was treated with the kINPen. The treatment gap is 9 mm, and the feed gas is 3 SLM of dry argon containing 40 ppm ·NO.

3. Results and discussion

3.1 Directly using Henry's law

The most straightforward method of implementing species transfer between a gas and liquid phase in a computational model is by directly coupling the concentrations in both phases at the gas-liquid interface via Henry's law:

$$\frac{c_l}{c_g} = H^{cc} \quad \text{with} \quad H^{cc} = H^{cp} \cdot RT \tag{3}$$

Where H^{cc} is the dimensionless Henry's constant, R the gas constant (J/mol·K), and T the temperature (K). This method has been used in several published models, including by our group (16, 27-31). For mass conservation, it is necessary to additionally specify that the flux of species entering the liquid must also exit the gas phase at the interface, thus recalculating both c_l and c_g. To investigate how well this boundary condition can describe the dissolution of chemical species into a liquid, we need to compare computational results to experiments where liquid water was treated with a gas jet that contains a known amount of RONS, whose concentration is afterwards measured in the treated liquid.

Such an experiment was performed by Winter *et al.* (20), where they measured how much H_2O_2 was dissolved into an aqueous medium after treatment with argon containing a known amount of gaseous H_2O_2, using the kINPen plasma jet (without igniting the plasma), as also described above (see **Figure 1a**). We thus adapted our model to the setup used in (20). **Figure 2a** shows the resulting H_2O_2 density profile in both gas and liquid phase calculated by the model, while **Figure 2b** illustrates how well using Henry's law directly as boundary condition at the interface can replicate the measured dissolution of H_2O_2 into the treated liquid. Clearly, there is very good agreement between model and experiment. Notably, almost all H_2O_2 present in the feed gas dissolves into the liquid. To emphasize this, **Figure 2b** additionally shows the maximum amount of H_2O_2 that would physically be able to dissolve (i.e. if 100% of the gaseous H_2O_2 that entered the system was dissolved in the liquid). The reason for this is two-fold: (i) H_2O_2 has an extremely high solubility ($H^{cc} = 1.84 \times 10^6$, at 300K), and (ii) in this setup, the treated liquid has a large surface area through which the species can dissolve.
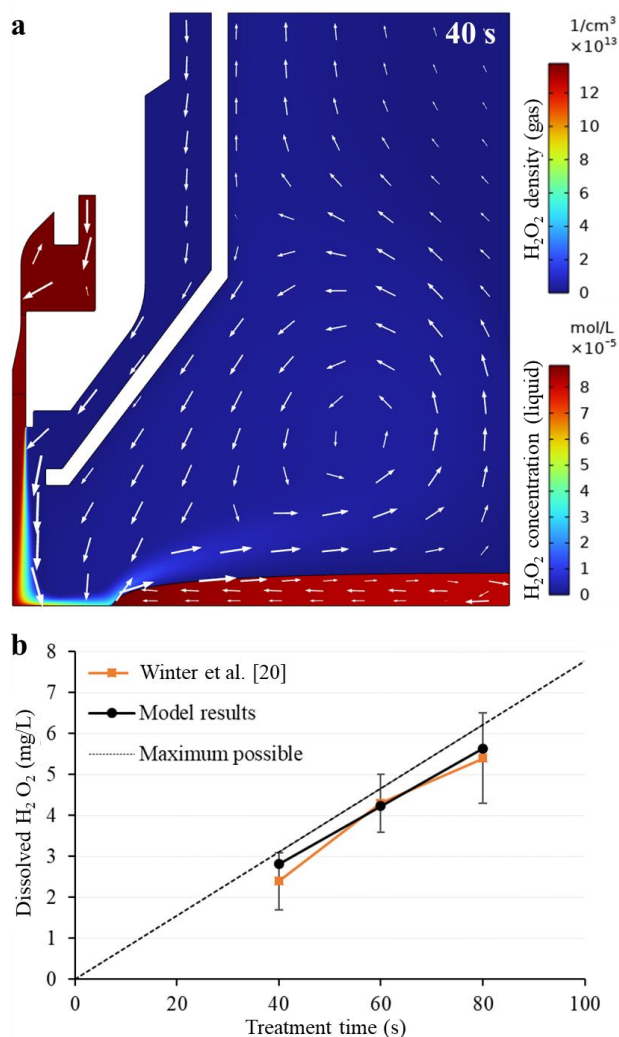
Figure 2: Model results for the setup geometry described in (20), where 5 mL of liquid is treated with 3 SLM of argon containing 5 ppm H_2O_2. (a) Calculated H_2O_2 density profile in gas and liquid phase, after 40 s of simulated treatment. Arrows represent the calculated flow field in the system. (b) Total dissolved H_2O_2 concentration over time, compared to the reported experimental data, and the maximum possible (see text).

Similar experiments were performed by Hassan *et al.* (21), though with a much higher gaseous H_2O_2 concentration, and a smaller liquid volume. In this case, as can be calculated from their reported data, a smaller fraction of the gaseous H_2O_2 dissolved into the treated liquid. **Figure 3** shows our simulation results when we adapt our model to their setup. **Figure 3a** depicts the calculated H_2O_2 density profile in gas and liquid phase. Just above the interface, the gaseous H_2O_2 is depleted (see inset in the figure) because of its high solubility, a phenomenon that has also been reported elsewhere (16, 17). Again, as seen in **Figure 3b**, our calculated amount of dissolved H_2O_2 agrees very well with the reported experimental values.

In the same work, Hassan *et al.* (21) also investigated the dissolution of O_3 into the treated liquid. In contrast to H_2O_2, O_3 has a low solubility ($H^{cc} = 0.24$, at 300K), inhibiting the depletion of the gas phase directly above the liquid, as visible in **Figure 3c**. **Figure 3d** shows that, unlike for H_2O_2, our model results now vastly overestimate how much O_3 dissolves into the liquid. In addition, our model predicts a significant change in dissolved amount depending on the liquid volume, while the experiments show no difference as

long as the surface area stays the same (note that the y-axis depicts the number of moles, not the concentration like in **Figure 2b**).
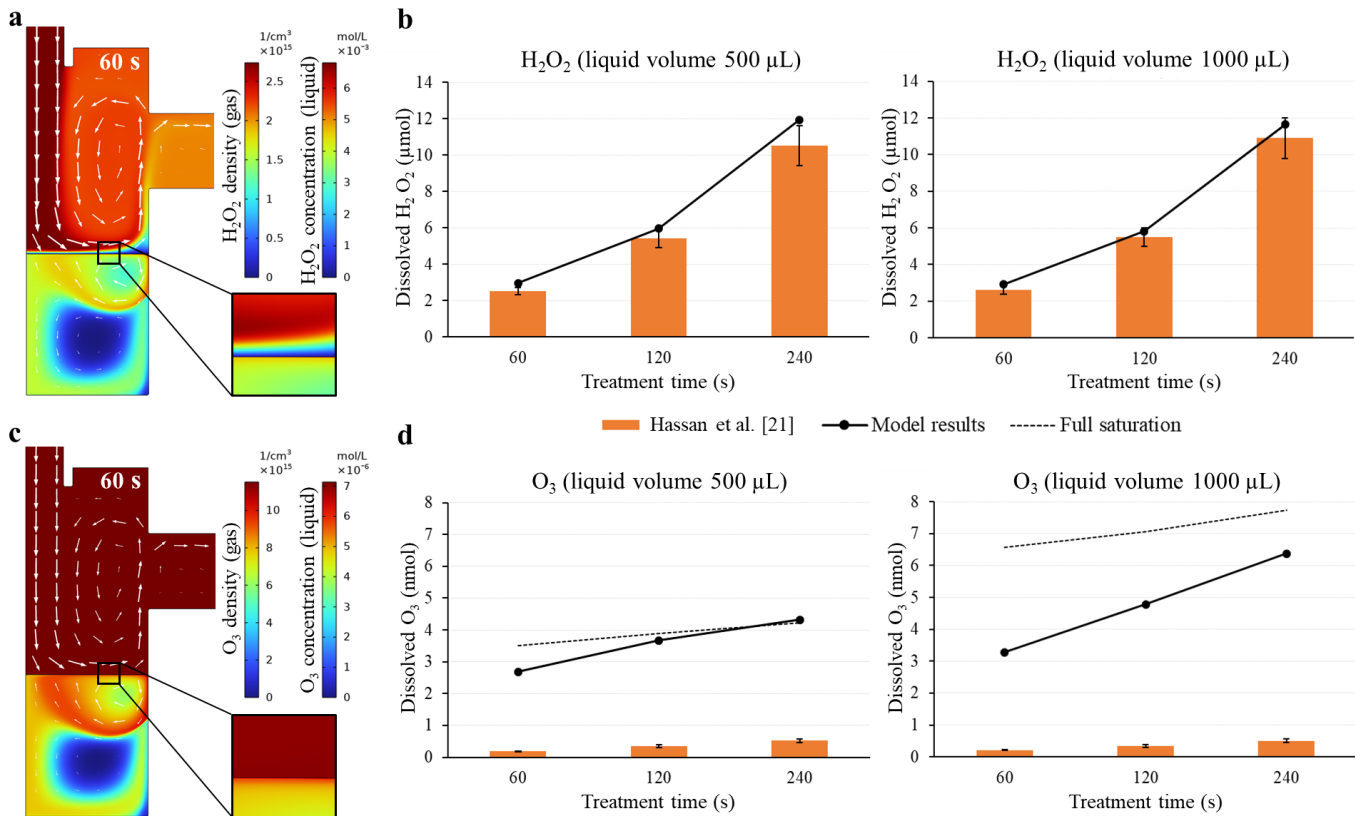

Figure 3: Model results for the setup geometry described in (21), where 500 µL and 1000 µL of liquid is treated with air containing either 110 ppm H_2O_2 (a, b) or 450 ppm O_3 (c, d). (a) Calculated H_2O_2 and (c) O_3 density profile in gas and liquid phase, after 60 s of simulated treatment. Arrows represent the calculated flow fields. (b, d) Total dissolved amount of H_2O_2 and O_3 over time, compared to the reported experimental data. For O_3, the total dissolved amount if the liquid were fully saturated when in contact with 450 ppm gaseous O_3 is also shown (dashed line). The saturated amount rises with time because the gas flow causes the liquid to cool: as we apply the temperature-dependent Henry's constants, the solubility thus increases with decreasing temperature.

From the above, it is clear that using Henry's law directly as the boundary condition governing species dissolution in the model is sufficient for highly soluble species, such as H_2O_2, but severely overestimates the dissolution of species with low solubility, such as O_3. The issue lies in the fact that by applying Henry's law directly, the model forces equilibrium at the interface in each time step, without taking into account how long it would take in reality to reach equilibrium. This causes the interface region to be saturated almost immediately, while the flow field continuously renews the liquid at the interface. For species with low solubility, this in turn causes the entire liquid phase to reach saturation soon, more so for smaller liquid volumes, as dissolved species are efficiently transported toward the bulk through convection. This is also visible in **Figure 3d**, when comparing the dissolved amount of O_3 over time calculated by our model with the dissolved amount if the liquid were saturated with O_3.

3.2 Other formulas used in literature

Clearly, a model that directly applies Henry's law does not produce correct results for the dissolution of gaseous (plasma-produced) species into liquid water. Although several published modelling studies have used Henry's law directly at the plasma-liquid interface, including our group (16, 27-31), many multi-dimensional models for plasma treatment of water have been reported over the past decade that take a different approach to describe the dissolution of neutral species. Numerous different formulas have been described in these works, but most can be grouped into either kinetic boundary conditions (32-34), diffusive boundary conditions (17, 35-41), or film theory (18). In the following, a recently reported use of each approach is briefly described.

The kinetic approach, as explained by Hassan *et al.* (21), treats the transfer of species between the gas and liquid phase with a flux Γ, based on the mean molecular velocity $\bar{v}$ of gas phase species above the interface:

$$\Gamma_{g \leftrightarrow l} = \frac{1}{4} \bar{v} \left(c_g - \frac{c_l}{H^{cc}} \right) \tag{4}$$

The above expression arises from the assumption that all gas molecules that strike the interface via random motion are transported to the liquid, while transport back to the gas phase happens continuously with a rate that depends on the species' surface concentration.

The diffusive approach essentially describes diffusion of chemical species through the liquid interface, but with a weighted diffusion coefficient (e.g. for the plasma/gas phase: $D = D_g \left(\frac{H^{cc} \cdot c_g - c_l}{H^{cc} \cdot c_g} \right)$) that depends on how close the system is to the equilibrium prescribed by Henry's law. In this way, Kruszelnicki *et al.* (17) applied two fluxes to the plasma-liquid interface in their model., i.e. a flux from gas to liquid, and a flux from liquid to gas:

$$\begin{cases} \Gamma_{g \to l} = \dfrac{D_g}{\Delta x} \left(\dfrac{H^{cc} \cdot c_g - c_l}{H^{cc} \cdot c_g} \right) (c_g - c_l) & \text{if } c_l < H^{cc} \cdot c_g \\[2ex] \Gamma_{l \to g} = \dfrac{D_l}{\Delta x} \left(\dfrac{c_l - H^{cc} \cdot c_g}{c_l} \right) (c_l - c_g) & \text{if } c_l > H^{cc} \cdot c_g \end{cases} \tag{5}$$

Here, Δx represents the mesh element size at the interface, taken in (17) to be 1 μm.

Finally, film theory describes a laminar "film" at the liquid interface through which the chemical species diffuse into and out of the liquid phase (42). If a film is assumed only on the liquid phase side of the interface, the flux between the two phases can be described as:

$$\Gamma_{g \leftrightarrow l} = \frac{D_l}{\Delta x} \left(H^{cc} \cdot c_g - c_l \right) \tag{6}$$

The above equation was employed in the context of plasma-liquid interaction by Semenov *et al.* (18), who assumed the film thickness, Δx, to be approximately equal to 10 μm. Each of the above boundary conditions prescribes a flux between the two phases that goes to zero as the system approaches Henry's law

equilibrium, but the magnitude of the fluxes differs for each formula. In case of **equation 5**, extra care must additionally be taken, as the flux also becomes zero for $c_g = c_l$, which is an unphysical equilibrium for all species that do not have a Henry's law constant equal to 1.

To investigate how **equations 4, 5 and 6** perform at replicating experimental results compared to directly applying Henry's law, we implemented them into our model. **Figure 4a** shows the results for H_2O_2. It can be seen that all curves overlap: regardless of the used boundary condition, the same amount of H_2O_2 is calculated to dissolve, which agrees very well with the experimental results. For O_3, as shown in **Figure 4b**, the results are similar for each equation used, though not identical, and comparable to when simply applying Henry's law directly. But, they are clearly higher than the experimental results. Hence, this means that all boundary conditions severely overestimate the amount of O_3 that dissolves into the treated liquid. The fact that different boundary conditions describing species dissolution behave similarly was also reported by Liu *et al.* (43), who compared the diffusive approach, kinetic approach and applying Henry's law directly (referred to there as the "thermodynamic" approach) in their 1D model. However, the authors did not compare the results to experiments. **Figure 4b** clearly illustrates that although these approaches indeed produce similar results, they are in fact wrong when compared with experiments.
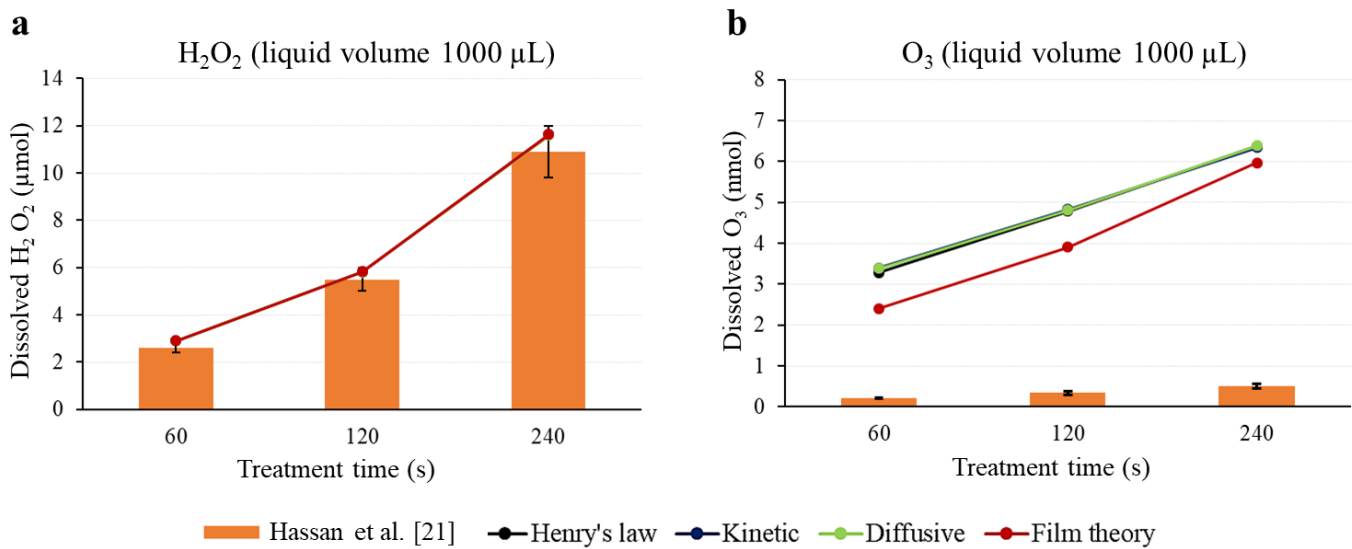

a H_2O_2 (liquid volume 1000 μL)

b O_3 (liquid volume 1000 μL)

Hassan et al. [21]   —●—Henry's law   —●—Kinetic   —●—Diffusive   —●—Film theory

Figure 4: Total dissolved amount of H_2O_2 (a) and O_3 (b) over time, as calculated by our model using four different boundary conditions on the gas-liquid interface, compared to the experimental data reported in (21). In (a), the four curves overlap, while in (b) the green, blue and black curve overlap.

The above essentially means that the different boundary conditions used in plasma-liquid literature overestimate the flux of plasma-produced species into the liquid. For species with high solubility like H_2O_2, this does not cause a problem. Its high solubility causes the gaseous region above the liquid to become depleted, meaning that transport from the "bulk" of the gas to the liquid surface is rate-limiting, not the transport of species into the liquid. For species with low solubility, the transport into the liquid is rate-limiting, so an overestimation of the flux across the interface causes overestimation of the dissolved amount. When directly applying Henry's law, this overestimation is caused by the assumption that equilibrium at the interface is reached instantly. For the kinetic and diffusive approach, transport from gas

to liquid is only determined through transport from the bulk gas to the interface (through $\bar{v}$ and D_g, respectively), in practice also causing equilibrium to be reached almost instantly. Only when applying film theory, the transport is limited by the resistance a species would encounter caused by transport into the liquid phase. More specifically, the flux from gas to liquid is determined by the transport from the interface to the bulk liquid (via D_l), and the concentrations at the interface evolve towards equilibrium over time, not near-instantly. Indeed, **Figure 4b** shows that when using film theory, the results lie (slightly) closer to the experimental values. However, the dissolved amount of O_3 is still severely overestimated.

3.3 Can we reach better agreement?

Describing the dissolution of chemical species into liquid water is, of course, not only relevant for plasma-liquid interaction. Other research fields, such as water purification and atmospheric chemistry, also describe the interaction of gas and liquid. In context of the latter, Kolb et al. (44) reviewed the different transport processes occurring near the gas-liquid interface. One aspect of this, which is not present in the formulas tested so far, is the accommodation of species at the gas-liquid interface. In a non-reactive setting, a gaseous molecule that strikes a liquid surface can either be reflected, or be accommodated and transferred through the interface. The ratio of these two outcomes is determined via the bulk mass accommodation coefficient, α_b, described as the probability for a molecule that strikes the liquid surface to actually enter the bulk liquid. As such, α_b determines the maximum possible flux of gaseous species into the liquid (45). In other words, besides transport from the gas bulk to the interface and transport from the interface to the bulk liquid, transport through the interface itself forms an additional barrier. In principle, not taking α_b into account is the same as assuming it has a value of 1, i.e. 100% of the species that follow the flux prescribed by the boundary condition at the gas-liquid interface will indeed be transported through the interface. Unfortunately, taking the mass accommodation coefficient into account is not straightforward. Most critical is the fact that values of α_b have been reported for only a handful of species, including only a few RONS, as previously also noted by Kruszelnicki *et al.* (17). Secondly, for the cases where data is available, reported values span several orders of magnitude for the same species. In theory, molecular dynamics simulations should be able to predict the mass accommodation coefficient of chemical species, but this approach has so far faced issues in reaching agreement with experiments (46, 47). A compilation of available data can be found in the Chemical Kinetics and Photochemical Data compilation by Burkholder *et al.*, NASA (48). Both H_2O_2 and O_3 are among the species for which values of the mass accommodation coefficient are available, allowing us to test the effect of taking this coefficient into account on the model results. Combining both film theory and the mass accommodation coefficient gives us the following boundary condition for the gas-liquid interface:

$$\Gamma_{g\leftrightarrow l} = \alpha_b \cdot \frac{D_l}{\Delta x}\left(H^{cc} \cdot c_g - \bar{c_l}\right) \tag{7}$$

Here, $\bar{c_l}$ is the average concentration in the liquid phase. In film theory, $\bar{c_l}$ should in principle be the concentration in the liquid bulk (42), but as our multidimensional model describes a finite liquid phase in which there is constant transport through convection, it is not possible to define a bulk concentration, which can instead be approximated by the average concentration. The maximum film thickness can be estimated as $\Delta x = \sqrt{2 \cdot D_l \cdot r / \bar{v}_{int}}$ where r is the radial dimension of the gas-liquid interface and $\bar{v}_{int}$ the

average velocity at the interface, i.e. $r/\bar{v}_{int}$ is the total interaction time between a fluid element in the liquid and the gas phase. The film thickness will vary in the radial direction. We will assume this variation to be quasi-linear, allowing us to use the cylindrical average of Δx for simplicity.

For H_2O_2, using the reported room temperature value of α_b = 0.1 (48), our computational results using **equation 7** still agree well with experimental data, as visible in **Figure 5a**. Because of its high solubility, the mass accommodation coefficient has nearly no effect on the modelling results for H_2O_2: even for a lower value, such as α_b = 0.01, the results stay the same. For O_3, (48) recommends a lower limit of α_b = 0.01. As an upper limit, we can use α_b = 0.1, i.e., the highest reported value of α_b for O_3. **Figure 5b** shows that using **equation 7** as the boundary condition at the gas-liquid interface indeed dramatically improves the agreement between our model and the experimental data. Now, for α_b = 0.01 the dissolved amount of O_3 is slightly underestimated, which can be expected as this value is a lower limit, with the actual value most likely being higher. For α_b = 0.1, the dissolved amount of O_3 is again overestimated, though the agreement is still much better than that shown in **Figure 4b**. Note that, instead of combining it with film theory, α_b could in principle also be combined with either the diffusive or kinetic approach. The latter was done by Oinuma *et al*. (33), i.e. the only other reported use of α_b in context of plasma liquid modelling, to the best of our knowledge. However, this combination with either the diffusive or kinetic approach does not change the results of these approaches, because they already overestimate the rate of dissolution significantly more compared to film theory, as mentioned in **section 3.2**. In contrast, we can conclude that using α_b in combination with film theory can reach better agreement with experiments for species with low solubility.
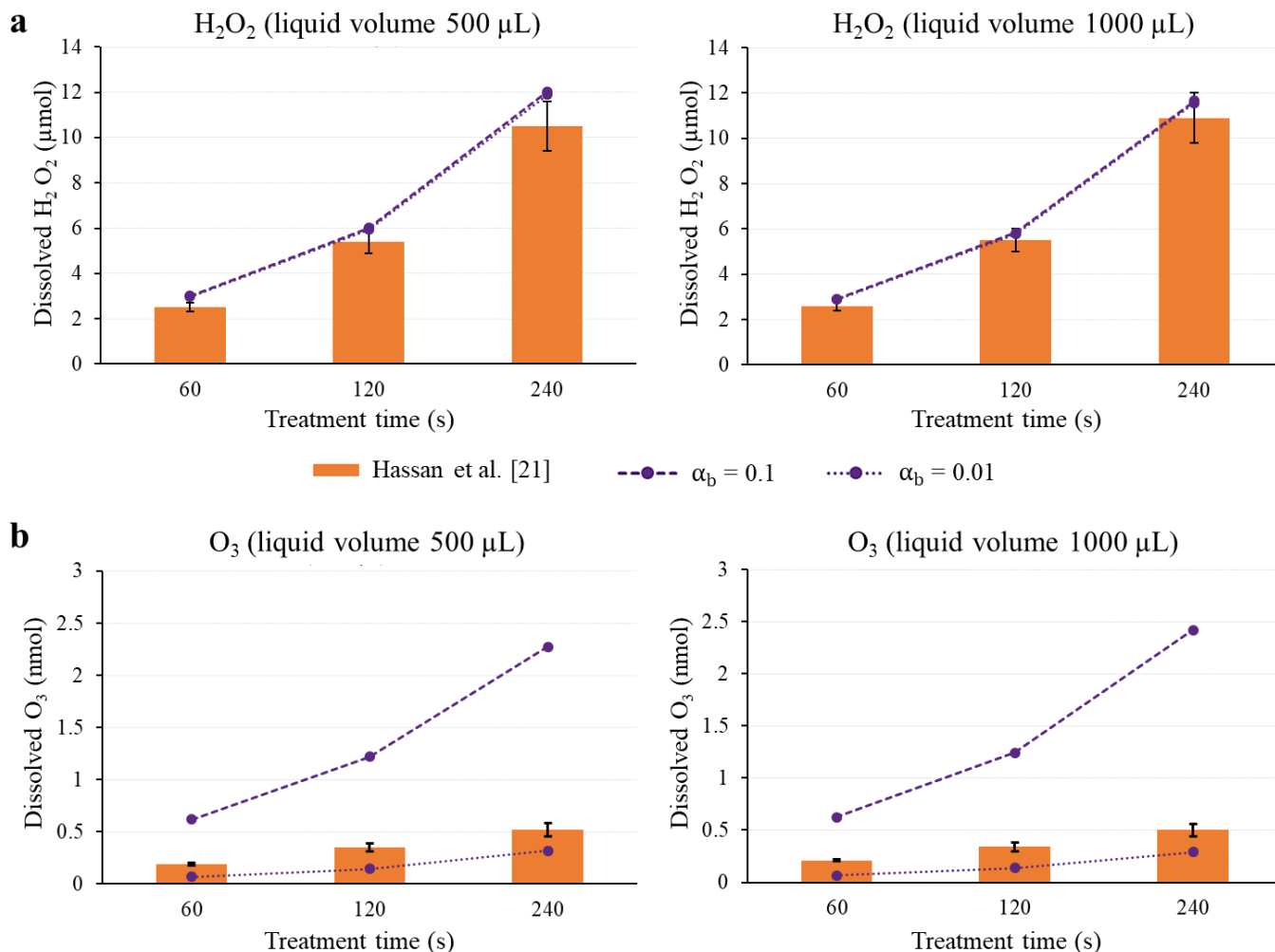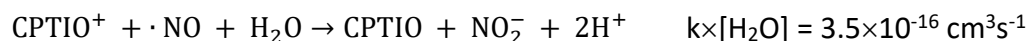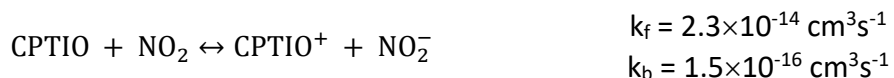
Figure 5: Total amount of dissolved H_2O_2 (a) and O_3 (b) over time, for a liquid volume of either 500 μL or 1000 μL, as calculated by our model using equation 7 as the boundary condition on the gas-liquid interface, for two values of α_b, compared to the experimental data reported in (21). In (a), both curves overlap.

3.4 Results in the presence of liquid phase reactions

So far, we have used experimental data where liquid water was treated with a gas jet that contains a known amount of RONS, whose concentration was afterwards measured in the treated liquid, for both a RONS with high solubility (H_2O_2) and low solubility (O_3). These RONS virtually do not react in the liquid. It would be beneficial to evaluate **equations 2, 4 – 6**, as well as whether **equation 7** performs better, for other RONS that do react in the liquid phase. Indeed, liquid phase reactions significantly affect the transport processes at the gas-liquid interface (19).

Jablonowski *et al.* (26) reported such experiment for ·NO, again a RONS with low solubility ($H^{cc} = 0.05$, at 300 K). Therefore, we adapted the geometry of our model again, to that used in (26). As the ·NO concentration was determined using a spin trap (CPTIO), this indeed allows to investigate our model results in the presence of chemical reactions. The reaction system for ·NO implemented into our model consists of the following reactions (49, 50):

$$CPTIO + \cdot NO \rightarrow CPTI + NO_2 \qquad\qquad k = 9.1\times10^{-18}\ cm^3s^{-1}$$

$$CPTIO + NO_2 \leftrightarrow CPTIO^+ + NO_2^- \qquad\qquad \begin{aligned} k_f &= 2.3\times10^{-14}\ cm^3s^{-1} \\ k_b &= 1.5\times10^{-16}\ cm^3s^{-1} \end{aligned}$$

$$CPTIO^+ + \cdot NO + H_2O \rightarrow CPTIO + NO_2^- + 2H^+ \qquad k\times[H_2O] = 3.5\times10^{-16}\ cm^3s^{-1}$$

By evaluating the CPTI concentration in this model, we can evaluate how well the dissolution of ·NO is simulated. Other reactions of ·NO in water, e.g. with O_2 or NO_2, are multiple orders of magnitude slower that the reaction with the spin trap at the conditions under study, and can thus be neglected here.

Secondly, Hassan et al. (25) recently published a follow-up to their earlier work, this time with experimental data for HNO_2. Compared to O_3 and H_2O_2, this species has a more intermediate solubility ($H^{cc} = 1.1 \times 10^3$, at 300 K). As HNO_2 dissociates in water, this again allows us to investigate the model results in the presence of chemical reactions, i.e.:

$$HNO_2 \leftrightarrow NO_2^- + H^+ \qquad\qquad pKa = 3.4$$

Unfortunately, no data is available regarding the mass accommodation coefficient of either ·NO or HNO_2. Meanwhile, fitting the model to find some optimal value of α_b would decrease its reliability and usability outside of the range of experimental parameters (in this case, the model geometry and precise chemical species) it was fitted to. Therefore, in first approximation, we test both the upper and lower limit used previously for O_3. Indeed, looking at the available values reported for different RONS, none are higher than $\alpha_b = 0.1$, and only few are lower than $\alpha_b = 0.01$ (48). Thus, when no data is available, this range seems a reasonable first approximation. **Figure 6** presents the results using this approach. Using Henry's law directly (**equation 2**), once again significantly overestimates the dissolution for both ·NO and HNO_2, though less severely than for O_3, which could be expected, as chemical reactions in the liquid in principle increase the effective solubility of the species (24). For HNO_2, which already has a higher solubility on its own, the overestimation is a factor ~2. Using **equation 7**, the upper limit of $\alpha_b = 0.1$ now approximates the measured values most closely, for both species. Notably, the experimental data in **Figure 6b** indicates that after 120 s treatment, more than double the amount of HNO_2 has dissolved compared to after 60 s, which is not predicted by the modelling results using **equation 7**. In fact, in the simulation results, a saturation effect can even be observed already, which does correspond well with the experimental results at 240 s. This is expected, as the dissolved amount of HNO_2 gets closer to its saturation concentration (i.e. 3560 nmol HNO_2 for the liquid volume of 500 µL). A possible explanation could be that the mass accommodation coefficient changes with the amount of HNO_2 already dissolved. Indeed, from reported data for HNO_3 it seems that α_b is higher for solutions that already contain HNO_3 compared to for pure water (48). However, as we have no data for the mass accommodation coefficient of HNO_2, this only remains speculative for now.
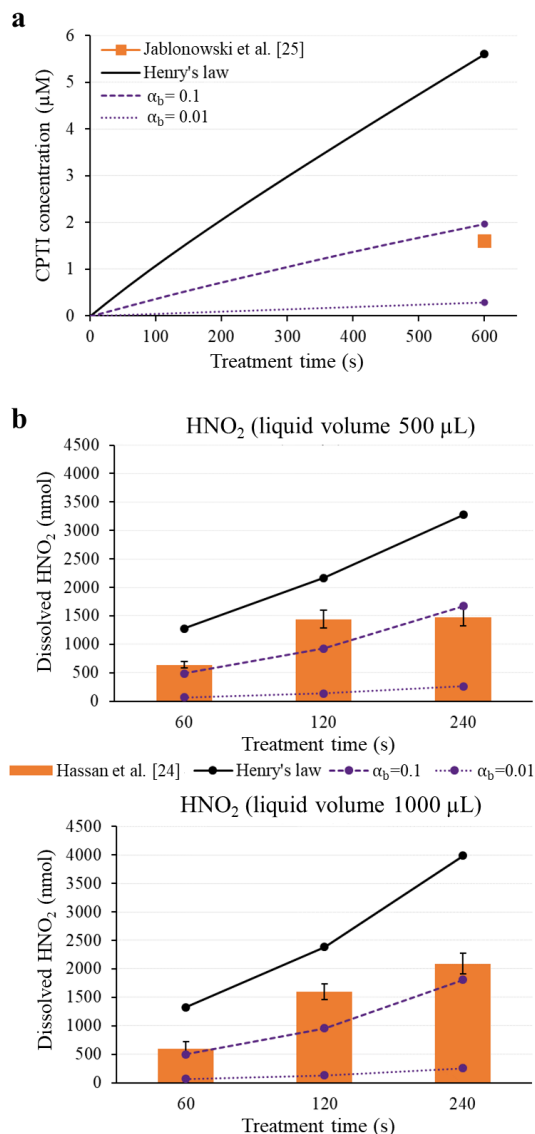
Figure 6: Model results for reacting systems in the liquid using either Henry's law directly, or equation 7 for two values of α_b as the boundary condition on the gas-liquid interface. (a) Total formed CPTI over time, formed through reaction of CPTIO with ·NO and thus a measure of the amount of dissolved ·NO. Modelling results are compared to the experimental data reported in (26). (b) Total amount of dissolved HNO_2 over time, for a liquid volume of either 500 µL or 1000 µL. Modelling results are compared to the experimental data reported in (25).

Taken together, our results indicate that many of the boundary conditions used in computational plasma-liquid research so far to describe the transfer of chemical species between the gas and liquid phase, are unable to reproduce experimental results for species with low solubility. By combining film theory and mass accommodation to describe transport at the interface, we reach a better agreement with experiments, at least for the RONS simulated in this work. One should note that **equation 7** is still a very simplified way of describing the dissolution process. Film theory was first proposed a century ago by Lewis and Whitman (51). Since then, it has been expanded into more sophisticated descriptions such as Danckwerts' surface renewal theory (52), or the resistance model, which more formally separates the

different transport processes near the interface (45). Implementation of more sophisticated descriptions could result in even better correlation with experimental values. However, the lack of data for the mass accommodation coefficient for many RONS remains an obstacle in reaching a robust description of the dissolution process in plasma-liquid research. Finally, it must be noted that the above discussion only applies directly to neutral RONS. For charged species, when actually included into the model, most works assume that the species are able to directly enter into the liquid phase without constraints (17, 28, 32, 36, 37, 39-41). It is difficult to test whether this approach is correct, as comparison to experimental data is not available for charged species. When the plasma is close to or in contact with the liquid, the transport of charged species towards the liquid can additionally be influenced by the electric field and the formed plasma sheath, further complicating the description of interfacial mass transport in plasma-liquid interaction (53).

4. Conclusion

In this work, we studied several interfacial boundary conditions to describe species transfer over the gas-liquid interface, as used in various published multidimensional plasma-liquid models. By comparing the results to experimental data, we show that the different expressions are unable to replicate measurements for all RONS. Specifically, we found that all formulas perform well for H_2O_2, which has high solubility, but severely overestimate the rate of dissolution for O_3, $\cdot NO$ and HNO_2, which have intermediate to low solubility. This discrepancy has likely gone unnoticed due to a lack in comparison between modelling results and experimental data for poorly soluble species. Indeed, rigorous benchmarking of different aspects of a computational model is crucial to increase confidence in the model, and thus improve our understanding of the simulated system. In the end, we propose a first step towards a more accurate description of species dissolution, by combining film theory with the mass accommodation coefficient, for improved multidimensional computational modelling. We hope that this work can be used to investigate and enhance the description of RONS dissolution into water during plasma-liquid interaction even more in the future.

Appendix

In a computational model to investigate plasma-liquid interaction, the velocity field in the simulated system is crucial for the spatial transport of chemical species in both the gas and liquid phase. Indeed, the velocity field greatly affects transport of gaseous species over the gas-liquid interface, as it can transport species away from the interface towards the liquid bulk more efficiently than would occur solely through diffusion (27). To confirm that our description of the liquid velocity field, in particular the way it is set in motion by the shear stress exerted on it by the flowing gas, is correct, we performed simulations based on the experimental work by Stancampiano *et al.* (23) Here, the authors treated a 0.5% starch solution with a helium plasma at a flow rate of 1 SLM, allowing for visualization of the velocity field by addition of KI to the liquid.

To mimic the conditions in these experiment, we adapted our model to the conditions used in (23). The results of these simulations are shown below.
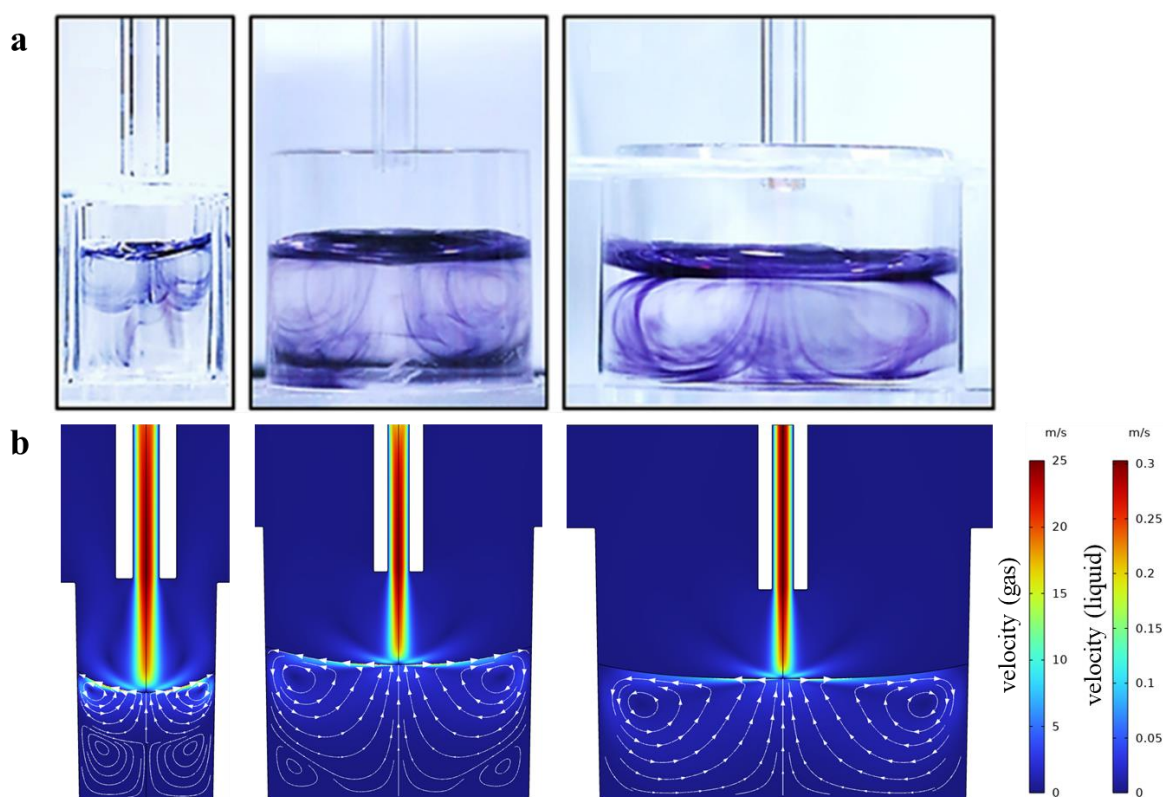

Figure A1: Experimentally determined liquid flow fields as reported in (23) (a), compared to the calculated flow fields predicted by our model for the same geometries and conditions (b). Adopted from (23) with permission from Institute of Physics and the authors.

We can see that the velocity fields calculated in our model qualitatively agree well with those observed in (23). Moreover, the maximum velocity of the liquid at the interface, under influence of the shear stress exerted by the flowing gas, is 0.3 m/s. This also falls in the range predicted by (23). Based on these simulations, we believe that the description of the velocity field in our modelling approach is sufficiently accurate, and thus so is its influence on the transport of chemical species throughout the simulated system.

References

1.   Huang Z, Xiao A, Liu D, Lu X, Ostrikov K. Plasma-water-based nitrogen fixation: Status, mechanisms, and opportunities. Plasma Processes and Polymers. 2022;19(4):2100198.
2.   Foster JE. Plasma-based water purification: Challenges and prospects for the future. Physics of Plasmas. 2017;24(5).
3.   Biondo O, Tomei G, Saleem M, Sretenović GB, Magarotto M, Marotta E, et al. Products, reactive species and mechanisms of PFOA degradation in a self-pulsing discharge (SPD) plasma reactor. Chemosphere. 2023;341:139972.
4.   Taghvaei H, Kondeti V, Bruggeman PJ. Decomposition of crystal violet by an atmospheric pressure RF plasma jet: the role of radicals, ozone, near-interfacial reactions and convective transport. Plasma Chemistry and Plasma Processing. 2019;39:729-49.
5.   Jablonowski H, von Woedtke T. Research on plasma medicine-relevant plasma–liquid interaction: what happened in the past five years? Clinical Plasma Medicine. 2015;3(2):42-52.
6.   Wende K, von Woedtke T, Weltmann K-D, Bekeschus S. Chemistry and biochemistry of cold physical plasma derived reactive species in liquids. Biological Chemistry. 2019;400(1):19-38.
7.   Dubuc A, Monsarrat P, Virard F, Merbahi N, Sarrette J-P, Laurencin-Dalicieux S, et al. Use of cold-atmospheric plasma in oncology: A concise systematic review. Therapeutic advances in medical oncology. 2018;10:1758835918786475.
8.   Tornin J, Labay C, Tampieri F, Ginebra M-P, Canal C. Evaluation of the effects of cold atmospheric plasma and plasma-treated liquids in cancer cell cultures. Nature Protocols. 2021;16(6):2826-50.
9.   Gorbanev Y, O'Connell D, Chechik V. Non-thermal plasma in contact with water: The origin of species. Chemistry–A European Journal. 2016;22(10):3496-505.
10.   Bruggeman PJ, Kushner MJ, Locke BR, Gardeniers JG, 981 07, Sweden, Graham W, Graves DB, et al. Plasma–liquid interactions: a review and roadmap. Plasma sources science and technology. 2016;25(5):053002.
11.   Kovačević VV, Sretenović GB, Slikboer E, Guaitella O, Sobota A, Kuraica MM. The effect of liquid target on a nonthermal plasma jet—imaging, electric fields, visualization of gas flow and optical emission spectroscopy. Journal of Physics D: Applied Physics. 2018;51(6):065202.
12.   Hansen L, Schmidt-Bleker A, Bansemer R, Kersten H, Weltmann K-D, Reuter S. Influence of a liquid surface on the NOx production of a cold atmospheric pressure plasma jet. Journal of Physics D: Applied Physics. 2018;51(47):474002.
13.   Samukawa S, Hori M, Rauf S, Tachibana K, Bruggeman P, Kroesen G, et al. The 2012 plasma roadmap. Journal of Physics D: Applied Physics. 2012;45(25):253001.
14.   Adamovich I, Baalrud S, Bogaerts A, Bruggeman P, Cappelli M, Colombo V, et al. The 2017 Plasma Roadmap: Low temperature plasma science and technology. Journal of Physics D: Applied Physics. 2017;50(32):323001.
15.   Adamovich I, Agarwal S, Ahedo E, Alves LL, Baalrud S, Babaeva N, et al. The 2022 Plasma Roadmap: low temperature plasma science and technology. Journal of Physics D: Applied Physics. 2022;55(37):373001.
16.   Verlackt C, Van Boxem W, Bogaerts A. Transport and accumulation of plasma generated species in aqueous solution. Physical Chemistry Chemical Physics. 2018;20(10):6845-59.
17.   Kruszelnicki J, Lietz AM, Kushner MJ. Atmospheric pressure plasma activation of water droplets. Journal of Physics D: Applied Physics. 2019;52(35):355207.
18.   Semenov I, Weltmann K, Loffhagen D. Modelling of the transport phenomena for an atmospheric-pressure plasma jet in contact with liquid. Journal of Physics D: Applied Physics. 2019;52(31):315203.
19.   Sander R. Compilation of Henry's law constants (version 5.0. 0) for water as solvent. Atmospheric Chemistry and Physics. 2023;23(19):10901-2440.
20.   Winter J, Tresp H, Hammer M, Iseni S, Kupsch S, Schmidt-Bleker A, et al. Tracking plasma generated H2O2 from gas into liquid phase and revealing its dominant impact on human skin cells. Journal of Physics D: Applied Physics. 2014;47(28):285401.
21.   Hassan ME, Janda M, Machala Z. Transport of gaseous hydrogen peroxide and ozone into bulk water vs. electrosprayed aerosol. Water. 2021;13(2):182.

22.   Heirman P, Verloy R, Baroen J, Privat-Maldonado A, Smits E, Bogaerts A. Liquid treatment with a plasma jet surrounded by a gas shield: effect of the treated substrate and gas shield geometry on the plasma effluent conditions. Journal of Physics D: Applied Physics. 2023;57(11):115204.

23.   Stancampiano A, Bocanegra PE, Dozias S, Pouvesle J-M, Robert E. Evidence, origin and impact of liquid flows in plasma medicine in vitro treatments with APPJs. Plasma Sources Science and Technology. 2021;30(1):015002.

24.   Smith FL, Harvey AH. Avoid common pitfalls when using Henry's law. Chemical engineering progress. 2007;103(9):33-9.

25.   Hassan ME, Janda M, Machala Z. Comparison of the Transport of Reactive Nitrogen Plasma Species into Water Bulk vs. Aerosolized Microdroplets. Plasma Chemistry and Plasma Processing. 2024:1-29.

26.   Jablonowski H, Schmidt-Bleker A, Weltmann K-D, von Woedtke T, Wende K. Non-touching plasma–liquid interaction–where is aqueous nitric oxide generated? Physical Chemistry Chemical Physics. 2018;20(39):25387-98.

27.   Lindsay A, Anderson C, Slikboer E, Shannon S, Graves D. Momentum, heat, and neutral mass transport in convective atmospheric pressure plasma-liquid systems and implications for aqueous targets. Journal of Physics D: Applied Physics. 2015;48(42):424007.

28.   Chen C, Liu D, Liu Z, Yang A, Chen H, Shama G, et al. A model of plasma-biofilm and plasma-tissue interactions at ambient pressure. Plasma Chemistry and Plasma Processing. 2014;34:403-41.

29.   Heirman P, Van Boxem W, Bogaerts A. Reactivity and stability of plasma-generated oxygen and nitrogen species in buffered water solution: a computational study. Physical Chemistry Chemical Physics. 2019;21(24):12881-94.

30.   Bissonnette-Dulude J, Heirman P, Coulombe S, Bogaerts A, Gervais T, Reuter S. Coupling the COST reference plasma jet to a microfluidic device: a computational study. Plasma Sources Science and Technology. 2024;33(1):015001.

31.   Liu Y, Peng W, Liu D, Fu F. Comparison of the transportation of reactive species from He and Ar atmospheric-pressure plasma jets to aqueous solutions. Journal of Physics D: Applied Physics. 2024.

32.   Ikuse K, Hamaguchi S. Roles of the reaction boundary layer and long diffusion of stable reactive nitrogen species (RNS) in plasma-irradiated water as an oxidizing media—numerical simulation study. Japanese Journal of Applied Physics. 2022;61(7):076002.

33.   Oinuma G, Nayak G, Du Y, Bruggeman PJ. Controlled plasma–droplet interactions: a quantitative study of OH transfer in plasma–liquid interaction. Plasma Sources Science and Technology. 2020;29(9):095002.

34.   Nayak G, Oinuma G, Yue Y, Sousa JS, Bruggeman PJ. Plasma-droplet interaction study to assess transport limitations and the role of· OH, O·, H·, O2 (a 1Δg), O3, He (23 S) and Ar (1s 5) in formate decomposition. Plasma Sources Science and Technology. 2021;30(11):115003.

35.   Mohades S, Lietz AM, Kruszelnicki J, Kushner MJ. Helium plasma jet interactions with water in well plates. Plasma Processes and Polymers. 2020;17(3):1900179.

36.   Ning W, Lai J, Kruszelnicki J, Foster JE, Dai D, Kushner MJ. Propagation of positive discharges in an air bubble having an embedded water droplet. Plasma Sources Science and Technology. 2021;30(1):015005.

37.   Norberg SA, Tian W, Johnsen E, Kushner MJ. Atmospheric pressure plasma jets interacting with liquid covered tissue: touching and not-touching the liquid. Journal of Physics D: Applied Physics. 2014;47(47):475203.

38.   Parsey G, Lietz AM, Kushner MJ. Guided plasma jets directed onto wet surfaces: angular dependence and control. Journal of Physics D: Applied Physics. 2020;54(4):045206.

39.   Tian W, Kushner MJ. Atmospheric pressure dielectric barrier discharges interacting with liquid covered tissue. Journal of Physics D: Applied Physics. 2014;47(16):165201.

40.   Tian W, Kushner MJ. Long-term effects of multiply pulsed dielectric barrier discharges in air on thin water layers over tissue: stationary and random streamers. Journal of Physics D: Applied Physics. 2015;48(49):494002.

41.   Tian W, Lietz AM, Kushner MJ. The consequences of air flow on the distribution of aqueous species during dielectric barrier discharge treatment of thin water layers. Plasma Sources Science and Technology. 2016;25(5):055020.

42.   Beltran FJ. Ozone reaction kinetics for water and wastewater systems: crc Press; 2003.

43.   Liu Y, Liu D, Zhang J, Sun B, Luo S, Zhang H, et al. Fluid model of plasma–liquid interaction: The effect of interfacial boundary conditions and Henry's law constants. AIP Advances. 2021;11(5).

44.   Kolb C, Cox RA, Abbatt J, Ammann M, Davis E, Donaldson D, et al. An overview of current issues in the uptake of atmospheric trace gases by aerosols and clouds. Atmospheric Chemistry and Physics. 2010;10(21):10561-605.

45.   Davidovits P, Kolb CE, Williams LR, Jayne JT, Worsnop DR. Update 1 of: Mass Accommodation and Chemical Reactions at Gas–Liquid Interfaces. Chemical Reviews. 2011;111(4).

46.   Garrett BC, Schenter GK, Morita A. Molecular simulations of the transport of molecules across the liquid/vapor interface of water. Chemical reviews. 2006;106(4):1355-74.

47.   Morita A, Garrett BC. Molecular theory of mass transfer kinetics and dynamics at gas–water interface. Fluid dynamics research. 2008;40(7-8):459.

48.   Burkholder J, Sander S, Abbatt J, Barker J, Cappa C, Crounse J, et al. Chemical kinetics and photochemical data for use in atmospheric studies; evaluation number 19. Pasadena, CA: Jet Propulsion Laboratory, National Aeronautics and Space …; 2020.

49.   Hogg N. Detection of nitric oxide by electron paramagnetic resonance spectroscopy. Free Radical Biology and Medicine. 2010;49(2):122-9.

50.   Goldstein S, Russo A, Samuni A. Reactions of PTIO and carboxy-PTIO with· NO,· NO2, and O 2.⁻. Journal of Biological Chemistry. 2003;278(51):50949-55.

51.   Lewis WK, Whitman WG. Principles of gas absorption. Industrial & Engineering Chemistry. 1924;16(12):1215-20.

52.   Danckwerts P. Significance of liquid-film coefficients in gas absorption. Industrial & Engineering Chemistry. 1951;43(6):1460-7.

53.   Vanraes P, Bogaerts A. The essential role of the plasma sheath in plasma–liquid interaction and its applications—A perspective. Journal of Applied Physics. 2021;129(22).